ACS APPLIED MATERIALS & INTERFACES

Research Article

www.acsami.org

Designed Architecture of Multiscale Porous TiO_2 Nanofibers for Dye-Sensitized Solar Cells Photoanode

Sun Hye Hwang, Chanhoi Kim, Hee Song, Suim Son, and Jyongsik Jang*

World Class University (WCU) program of Chemical Convergence for Energy & Environment (C_2E_2), School of Chemical and Biological Engineering, Seoul National University, 599 Gwanangno, Gwanakgu, Seoul 151-742, Korea

Supporting Information

ABSTRACT: Multiscale porous (MSP) TiO_2 nanofibers (NFs) were fabricated using a simple electrospinning and etching process with TiO_2/SiO_2 composite NFs for high-efficiency dye-sensitized solar cells (DSSCs). TiO_2 NFs with different pore sizes (small, large, and multiscale) were prepared using SiO_2 nanoparticles of various sizes. The surface area of the MSP TiO_2 NFs was nine times higher than that of pristine TiO_2 NFs, providing sufficient dye adsorption for light harvesting as well as efficient paths for electrolyte contact. Moreover, the one-dimensional structure provides efficient light scattering and fast electron transport. As a result, DSSCs exhibited an enhanced current density (J_{sc}) of 16.3 mA cm^{-2} and a high photoconversion efficiency (η) of 8.5%, greater than those of conventional photoelectrodes made of TiO_2 nanoparticles (J_{sc} of 12.0 mA cm^{-2} and η of 6.0 %).

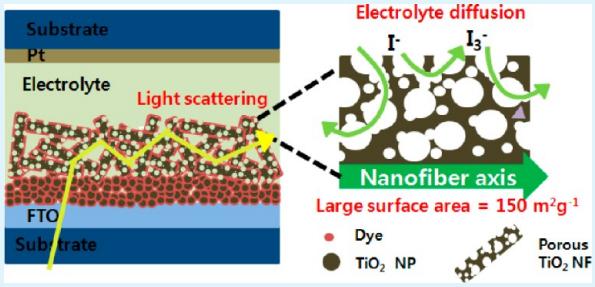

KEYWORDS: *porous TiO_2, TiO_2 nanofiber, light scattering, multifunctional TiO_2, dye-sensitized solar cell*

INTRODUCTION

Dye-sensitized solar cells (DSSCs) have been recognized as promising candidates for next-generation solar cells.[1−3] Theoretical and experimental research has focused on their high power conversion efficiency of up to 11%,[4,5] whereas continuing efforts have been devoted to improving efficiency.[6−10] To enhance the efficiency of DSSCs, approaches such as a thin blocking layer on the anode electrode, various metal oxide material structures and TiO_2 film pore-size distributions, and $TiCl_4$ post-treatment on nanocrystalline TiO_2 have been developed.[11−18]

The structure of scattering materials has been studied because it confines incident light within an electrode, thus enhancing photocurrent density.[19−21] Koo et al. reported that hollow spherical TiO_2 nanoparticles could increase the efficiency of solar cells based on their high surface area and light-scattering effect.[22] However, although hollow TiO_2 nanoparticles have a high surface area for the attachment of dye molecules, structural disorder caused by the grain boundaries of adjacent nanoparticles leads to the loss of free electrons and reduced carrier mobility.[23−25] Joshi suggested the use of one-dimensional TiO_2 nanofibers (NFs) to enhance light harvesting and fast electron transport.[26] One-dimensional nanostructures, including NFs, nanowires, nanorods, and their composites with TiO_2 nanoparticles, could also improve the electron mobility and transport rate.[27−34] However, dye adsorption is expected to be much less for these one-dimensional structures than for nanoparticles owing to their lower surface area. In general, high specific surface area, pronounced light-scattering effects and facilitate electrolyte diffusion are critical for a high-performance photoanode, but these factors are often incompatible with one another. To achieve these characteristics, we propose a new multifunctional material that offers high surface area, strong light scattering, and circulation for electrolyte reduction.

We successfully fabricated multiscale porous (MSP) TiO_2 NFs using a simple electrospinning method. TiO_2 NFs were prepared with different pore sizes (small, large, and multiscale). Scheme 1 shows an illustration of the MSP NF-coated TiO_2 nanoparticle films. The surface area of the MSP TiO_2 NFs was nine times higher than that of the pristine TiO_2 nanofibers,

Scheme 1. Schematic Illustration of the 15−20 nm TiO_2 Nanoparticle (NP) Underlayer, the MSP TiO_2 NF Scattering Overlayer, And the Magnified Structure of MSP TiO_2 NFs

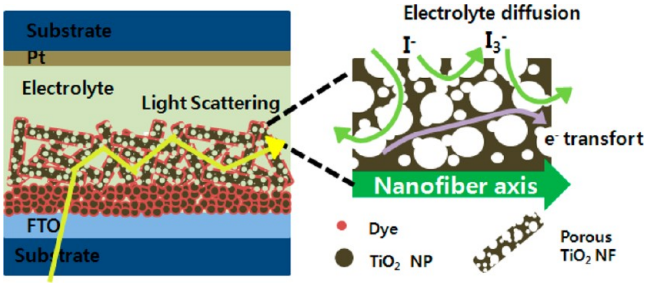

Received: July 5, 2012
Accepted: September 17, 2012
Published: September 17, 2012

which adsorbed a sufficient amount of dye for light harvesting. Moreover, after sunlight passed through the MSP TiO_2 NF layer, the remnant light could be scattered back for regeneration of dye molecules. Importantly, large pores in MSP TiO_2 NFs provided a place for circulation, facilitating electrolyte diffusion for oxidation reactions as shown in Scheme 1. Therefore, the MSP structure of TiO_2 NFs enabled sufficient dye adsorption, light scattering, and circulation of electrolyte. The efficiency of MSP TiO_2 DSSCs can be improved by 6.0–8.5%, which is indicative of ca. 42% over TiO_2 nanoparticles.

EXPERIMENTAL SECTION

Materials. Poly(vinylpyrrolidone) (PVP, M_w = 1 300 000), titanium isopropoxide (TTIP, $Ti\{OCH(CH_3)_2\}_4$), tetraethyl orthosilicate (TEOS, $Si(OC_2H_5)_4$) were purchased from Aldrich Chemical Co. TiO_2 nanoparticles (NPs) (Solaronix, Ti-Nanoxide T), *cis*-disothiocyanato-bis (2, 20-bipyridyl-4, 40-dicarboxylato) ruthenium-(II) bis(tetrabutylammonium) (N-719), and an iodide-based redox electrolyte (AN50) were purchased from Solaronix (Aubonne, Switzerland). FTO glass (15 Ω cm^{-2}, thickness of 2.2 mm) was obtained from Pilkington (Toledo, USA).

Preparation of Porous TiO_2 Nanofibers. SiO_2 nanoparticles were prepared via the Stöber method for fabrication of porous TiO_2 nanofibers (NFs).[35] A solution containing 148 mL of ethanol, 6 mL of ammonia solution, and 6 mL of tetraethyl orthosilicate was stirred for 12 h at 50°C to obtain a SiO_2 colloidal solution. The prepared SiO_2 solution was dispersed in 100 mL absolute ethanol. Then, 15 g poly(vinyl pyrrolidone) was dissolved in 100 mL of SiO_2 colloidal solution and stirred vigorously for 2 h. The final solution was prepared by dissolving various amounts of titanium isoproxide and acetic acid. The viscous hybrid solution was injected using a syringe. The diameter of the needle in the electrospinning was 0.1 mm, and the needle was conneted to the positive terminal of a power supply. The flow rate of the solution was 10 μL min^{-1}, controlled by a syringe pump purchased from KD Scientific (USA). A voltage of 10 kV was applied between the needle and the collector, which was grounded and used to collect the NFs at room temperature, and the distance between the nozzle and collector was 15 cm. The collector area was 600 cm^2. Next, the electrospun NFs were calcined at 500 °C for 6 h. The prepared SiO_2/TiO_2 NFs were etched by HF solution to obtain porous TiO_2 NFs.

Assembly of Dye-Sensitized Solar Cell. The TiO_2 film with double-layered structure was composed of the TiO_2 NP (15-20 nm) underlayer and the MSP TiO_2 NF overlayer. As a control, the film was prepared using only TiO_2 NPs with a diameter of ca. 15–20 nm. To prepare a mixture of MSP TiO_2 NFs and paste, we dispersed MSP TiO_2 NFs in anhydrous ethanol by sonication for 30 min before drying of MSP TiO_2 NFs. The samples within range of 0–22.5% were added to the paste and then mixed using a mortar and pestle. The paste was composed of 2.5 mL of terpineol, 0.1 g of ethyl cellulose, and 0.18 g of lauric acid. Fluorine-doped tin dioxide (FTO) glass substrates were cleaned by successive sonication in deionized water, acetone, and 2-propanol for 60 min each, and then treated with oxygen plasma for 30 s. Fluorine-doped tin oxide (FTO) glass substrate was pretreated with 40 mM $TiCl_4$ solution and heated at 450 °C for 30 min. A photoanode was prepared by applying the TiO_2 NPs underlayer and MSP TiO_2 NF overlayer onto the FTO substrate using a doctor blade. The photoanodes were sintered at 450 °C for 30 min, and then treated with $TiCl_4$ and sintered again as above. The resulting TiO_2 films were immersed in acetonitrile and tert-butanol (5:5 v/v) containing 5 × 10^{-4} M of N-719 and kept at room temperature for 36 h. Pt counter electrodes were prepared on the FTO glasses using 5 mM H_2PtCl_6 solution, followed by heating at 400°C for 30 min in air. In a sealed cell, iodide-based low-viscosity electrolyte with 50 mM tri-iodide, ionic liquid, lithium salt, and pyridine derivative in acetonitrile (AN50) was introduced.

Instrument. The morphology of porous TiO_2 NFs was investigated by field-emission scanning electron microscopy (FE-SEM) (JEOL 6700) and transmission electron microscopy (TEM) (JEOL JEM-200CX). X-ray diffraction (XRD) data were obtained using an M18XHF-SRA (Mac Science Co.) with a Cu Kα radiation source (λ = 1.5406 Å) at 40 kV and 300 mA (12 kW). BET surface areas of nanofibers were acquired using a Micromeritic analyzer (ASAP 2000, Micromeritic Co.) Diffuse reflectance spectra were measured by Lambda 1050 from PerkinElmer. The photocurrent–voltage (I–V) characteristics of the assembled DSSCs were evaluated using a 500 W xenon lamp (XIL model 05A50KS source units). The incident photon-to-current efficiency (IPCE, PV measurements, Inc.) was measured from 300 nm to 800 nm under under the global AM 1.5 solar emission spectrum.

RESULTS AND DISCUSSION

MSP TiO_2 NFs were fabricated by a simple electrospinning method. A mixed solution containing colloidal SiO_2 nanoparticles (20 nm), tetraethyl orthosilicate (TEOS), titanium isoproxide (TTIP), poly(vinyl pyrrolydone) (PVP), acetic acid, and absolute ethanol was jetted by a single spinneret. Electrospun NFs were calcined at 500 °C for 6 h, and and then the SiO_2 portion of the prepared SiO_2/TiO_2 composite (STC) NFs was etched with an HF solution which concentration was 0.42 wt % for 18 h. Finally, MSP TiO_2

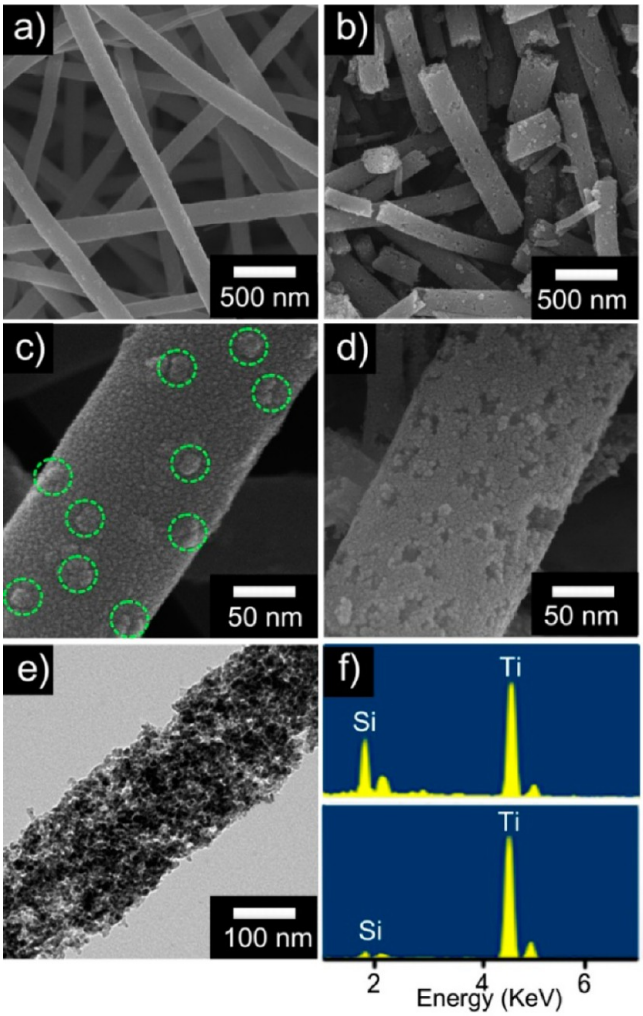

Figure 1. FE-SEM images of (a) SiO_2/TiO_2 composite nanofibers (STC NFs) and (b) MSP TiO_2 NFs. (c) High-magnification SEM image of an STC NF and (d) high-magnification SEM image of an MSP TiO_2 NF. TEM image of (e) MSP TiO_2 NF and (f) EDS data for the STC NFs (top) and MSP TiO_2 NFs (bottom).

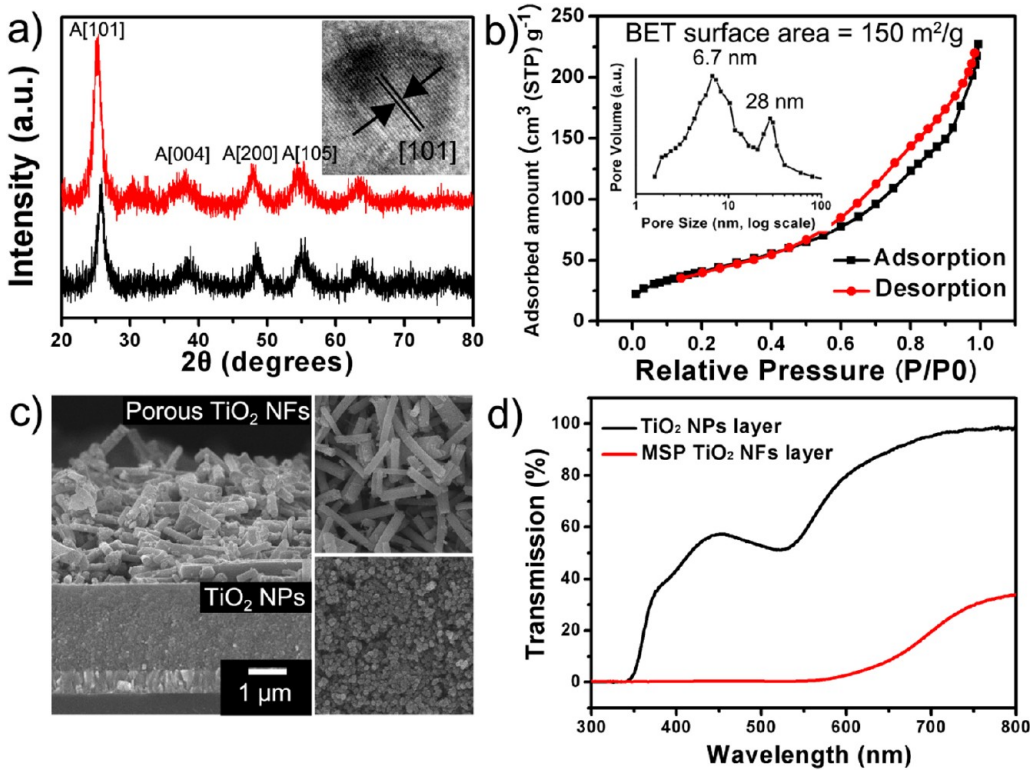

Figure 2. XRD patterns of (a) STC NFs (black) and MSP TiO_2 NFs (red). The letter "A" denotes peaks for the anatase phase, and the inset HR-TEM image shows *d*-spacing of the MSP TiO_2 NFs. (b) Nitrogen adsorption isotherm of the MSP TiO_2 NFs. (c) Cross-sectional SEM image of a double-layer structure with the TiO_2 NP (15−20 nm) underlayer and the MSP TiO_2 NF overlayer and surface SEM images for each layer. (d) Transmission spectrum for the 15-20 nm TiO_2 nanoparticle layer (black) and MSP TiO_2 NF layer (red) after dyeing at the same thickness.

NFs were fabricated. A field-emission scanning electron microscopy (FE-SEM) image of the STC NFs after calcination at 500°C for 6 h is shown in Figure 1a. The obtained STC NFs had diameters of 250 nm or larger and lengths greater than 50 μm. As shown in Figure 1b, the diameters of the prepared MSP TiO_2 NFs were the same as the STC NFs. However, the MSP TiO_2 NFs were shorter than the STC NFs due to HF etching. The high-resolution SEM image of STC NFs (Figure 1c) shows that SiO_2 nanoparticles were embedded in TiO_2 (the dashed circles indicate embedded SiO_2 nanoparticles). Figure 1d shows wormhole-like pores in the TiO_2 NFs, which originated from the removal of SiO_2 via HF etching. Figure 1e shows a transmission electron microscopy (TEM) image of an MSP TiO_2 NF. The TiO_2 NFs had an MSP structure that consisted of small pores due to TEOS (SiO_2 precursor) and large pores due to colloidal SiO_2 nanoparticles. The MSP TiO_2 NFs were made up of TiO_2 nanoparticles with an average diameter of ~10 nm. Energy-dispersive X-ray spectroscopy (EDS) results indicated that the atomic ratio of Si to Ti changed from 27:73 to 0.5:99.5 because of removal of SiO_2 by HF etching.

X-ray diffraction (XRD) analysis was performed to confirm the crystallization of MSP TiO_2 NFs. As shown in Figure 2a, XRD results showed that electrospun STC NFs (black) and MSP TiO_2 NFs (red) consisted of the anatase phase with an average diameter of approximately 10 nm. High-resolution transmission electron microscopy (HR-TEM) analysis was also used to investigate the crystalline phase of TiO_2 NFs. In the HR-TEM image in Figure 2a, a lattice spacing of 0.35 nm can be observed, implying the presence of anatase crystalline phase of TiO_2 [101] planes. The anatase phase of TiO_2 possesses a higher electron transport capability than the rutile phase, leading to better photovoltaic performance.[36] Figure 2b shows that the pore volume and Brunauer−Emmett−Teller (BET) surface areas of MSP TiO_2 NFs were 0.31 $cm^3\ g^{-1}$ and 150 $m^2\ g^{-1}$, respectively. The pore sizes of the MSP TiO_2 NFs were determined to be 6.7 nm by 28 nm by measuring the Barrett−Joyner−Halenda (BJH) pore distribution. Figure 2c shows SEM cross-sectional images of a double-layered structure (ca. 3 μm-thick TiO_2 nanoparticle layer (15−20 nm) and ca. 5 μm porous TiO_2 NFs [250 nm]) on the glass substrates. The well-defined shape, size, and uniformity of the nanoparticles and NFs are clearly observed. As shown in Figure 2d, the transmission of incident light in the range of 300−800 nm was investigated for single TiO_2 NPs layer and the double layer containing TiO_2 NPs and MSP TiO_2 NFs after dyeing. In case of single TiO_2 NPs layer, transmission of incident light at 750 nm was 97 %. At nearly 400 nm and 535 nm, decreased transmission in the curve was observed due to absorption of light by N-719 (Dye). On the other hand, the transmission of incident light in the range of 300−800 nm for the double layer containing TiO_2 nanoparticles and MSP TiO_2 NFs was significantly suppressed compared to a single TiO_2 NPs layer, indicating that the layer of MSP TiO_2 NFs was sufficient for light scattering and absorption in the range of 300−800 nm. Diffuse reflectance of TiO_2 NPs layer and MSP TiO_2 NFs layer with and without dye was also investigated to confirm light scattering effect (see Figure S1 in the Supporting Information). Light scattering depends on the size of NFs. Forward scattering increases with increasing fiber diameter, whereas backward scattering is negligible regardless of fiber diameter. Forward scattering intensity for the 200 nm NFs was relatively weak. When the diameters of the NFs increased to 200 nm or larger,

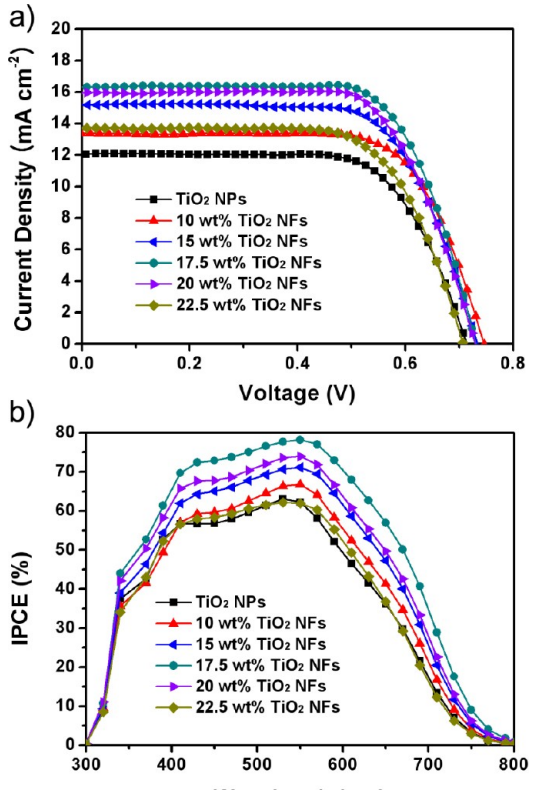

Figure 3. (a) Current density–voltage (J–V) curves and (b) incident photon-to-electron conversion efficiencies (IPCE) for the DSSCs fabricated from the double-layer structure of 10 nm nanoparticles and MSP TiO_2 NFs with different MSP TiO_2 NF/paste weight ratios.

Table 1. Summary of Photovoltaic Properties of the DSSCs with Photoanodes Containing Various MSP TiO_2 NFs[a]

	J_{sc} (mA cm^{-2})	V_{oc} (V)	FF (%)	η (%)	Thickness (μm)
TiO_2 NPs	12.0	0.71	69.5	6.0	8.0
10 wt % NFs	14.0	0.75	68.6	7.0	4.3
15 wt % NFs	15.2	0.73	68.8	7.7	6.8
17.5 wt % NFs	16.3	0.73	70.9	8.5	8.0
20 wt % NFs	16.0	0.72	69.3	8.1	9.2
22.5 wt % NFs	13.7	0.70	68.0	6.6	10.5

[a]Measurement were performed under AM 1.5G one sun light intensity of 100 W cm^{-2} and the active areas were about 0.25 cm^2 for all of the cells.

Table 2. Summary of photovoltaic properties of the DSSCs with photoanode containing different pore type of TiO_2 NFs[a]

	J_{sc} (mA cm^{-2})	V_{oc} (V)	FF (%)	η (%)	surface area (m^2 g^{-1})	adsorbed dye ($\times 10^{-6}$ mol g^{-1})
TiO_2 NPs	12.0	0.71	69.5	6.0		146.0
TiO_2 NFs	10.7	0.71	62.4	4.8	19	63.9
LP TiO_2 NFs	12.6	0.72	65.1	6.0	28	73.4
SP TiO_2 NFs	15.6	0.72	67.5	7.6	128	112.7
MSP TiO_2 NFs	16.3	0.73	70.9	8.5	150	132.7

[a]Measurements were performed under AM 1.5 G one sun light intensity of 100 W cm^{-2} and the active areas were about 0.25 cm^2 for all of the cells.

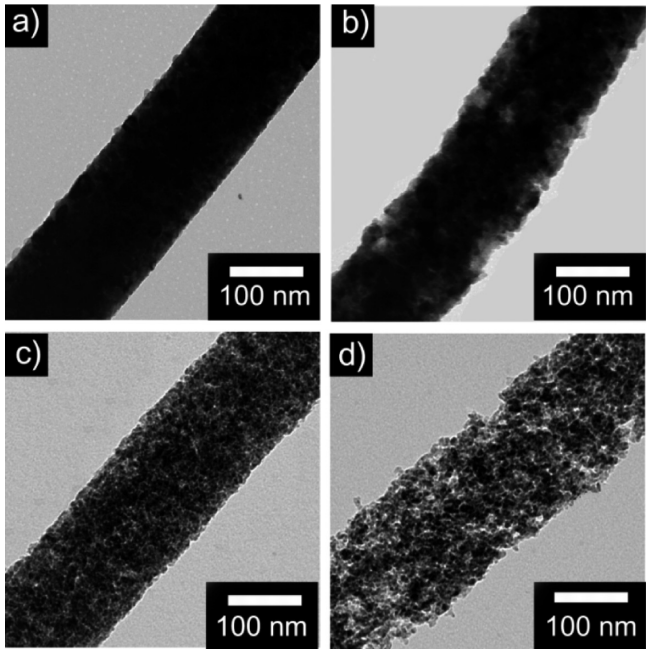

Figure 4. TEM images of (a) TiO_2 NFs, (b) LP TiO_2 NFs, (c) SP TiO_2 NFs, and (d) MSP TiO_2 NFs after HF etching.

the light scattering became substantially stronger.[37] Because the diameters of the MSP TiO_2 NFs were ca. 200–300 nm, these NFs induced strong light scattering and thereby enhanced light harvesting.

Figure 3a shows the dependence of current density–voltage curves (J–V curves) on the concentration of MSP TiO_2 NFs. The efficiency of DSSCs significantly increased with increasing MSP TiO_2 NF concentration up to 17.5 wt %. In particular, the solar cell device containing 17.5 wt % MSP TiO_2 NFs exhibited a short-circuit current density (J_{sc}) of 16.3 mA cm^{-2} and an energy conversion efficiency (η) of 8.5% (Figure 3a and Table 1). Compared to 17.5 wt % MSP TiO_2 NFs, the DSSC containing 10 wt % MSP TiO_2 NFs had J_{sc} and η values of 14.0 mA cm^{-2} and 7.0% (Figure 3a and Table 1). The thickness of the NF layer also increased with increasing MSP TiO_2 NF weight percent, leading to decrease open-circuit photovoltage (V_{oc}). A thicker film could provide a higher surface area for dye adsorption on the MSP TiO_2 NFs. However, when the amount of MSP TiO_2 NFs was greater than 17.5 wt %, the efficiency of the DSSC decreased significantly. The reason is that J_{sc} and V_{oc} decrease with increasing film thickness, due to augmentation of the surface area, which provides additional charge-recombination sites and enhances the dark current.[20] Moreover, a thick outer TiO_2 particle region does not contribute significantly to the photogeneration of conduction-band electrons due to light filtering by particles located close to the fluorinated tin oxide (FTO) glass. The DSSCs made using only TiO_2 nanoparticles had J_{sc} and η values of 12.0 mA cm^{-2} and 6.0 % (Figure 3a and Table 1). The J_{sc} of the MSP TiO_2 NFs was greater than that of the DSSC containing only TiO_2 nanoparticles, even though the TiO_2 film thicknesses were the same. As shown in the table 2, the amount of adsorbed dye on TiO_2 NPs is more than MSP

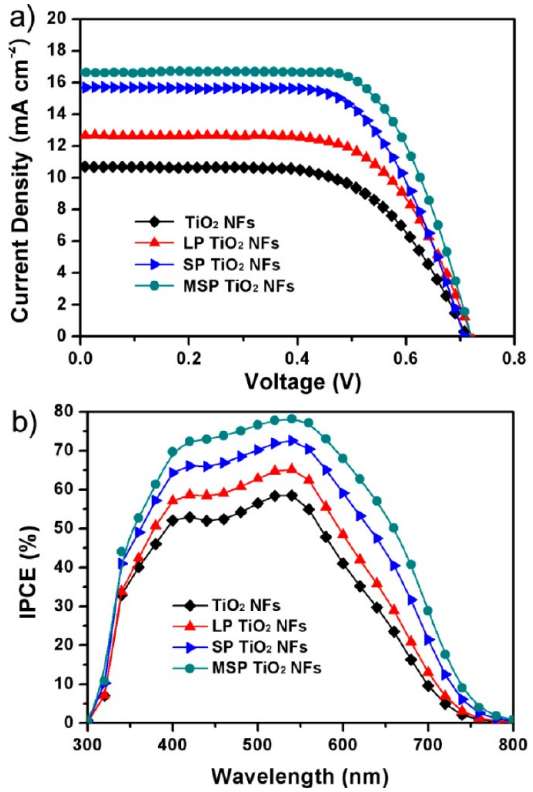

Figure 5. (a) Current density−voltage (J−V) curves. (b) Incident photon-to-electron conversion efficiencies (IPCE) for the DSSCs fabricated from the double-layer structure consisting of 10 nm nanoparticles and TiO_2 NFs with different pore sizes.

TiO_2 NFs. Judging from this data, the significant increase in J_{sc} is related to light scattering.[26,38]

Figure 3b indicates that incident photon-to-electron conversion efficiencies (IPCE) were greatly enhanced with increased MSP TiO_2 NF concentration. To confirm light scattering effect, the IPCE of MSP TiO_2 NFs content of 17.5 wt % was compared to only TiO_2 NPs. The quantum efficiency enhanced from 36% to 57% around 650 nm, which is indicative of ca. 57% over only TiO_2 nanoparticles. On the basis of these data, 79% of incident light in the visible region was easily absorbed by the MSP TiO_2 NF layer, leading to significant enhancement of the solar cell efficiency by strong light scattering.

Figure 4 shows the synthesized TiO_2 NFs with different pore types. The pore size of the TiO_2 NFs was controlled by the SiO_2 etching process (Figure 4a−d). In HF solution, silicon−oxygen bonding is broken by protonation of a surface oxygen atom bonded to the silicon atom (eq 1). Then, silicon−fluorine bonds form by nucleophilic attachment of HF^{2-} (or H_2F_2) to the electrophilic silicon atom (eq 2). Consequently, the silica part of the NFs was removed by HF treatment.[39]

$$\mathrm{Si-O-X+H^+ \rightarrow Si-O(H)+-X\ (X=Si\ or\ H)} \quad (1)$$

$$\mathrm{Si-O(H^+)-X+HF^{2-} \rightarrow Si-F+HO-X+HF} \quad (2)$$

The size of the SiO_2 region, formed by SiO_2 colloidal nanoparticles and SiO_2 precursor, plays a key role in the formation of various pore sizes. Large-pore (LP) TiO_2 NFs were prepared by removing SiO_2 colloidal nanoparticles, and small-pore (SP) TiO_2 NFs were prepared by removing small SiO_2 nanoparticles formed by the SiO_2 precursor. In addition, MSP TiO_2 NFs were obtained from SiO_2 colloidal nanoparticles and SiO_2 precursor containing the NFs (Figure 4a−d). Especially, among the TiO_2 NFs with different pore types, surface area of MPS TiO_2 NFs is largest. The polymer solution containing TiO_2 precursor, SiO_2 colloidal nanoparticles, and SiO_2 precursor was prepared by vigorously stirring. Under the vigorous stirring, SiO_2 precursor in polymer solution could disperse smaller droplet by collision between SiO_2 colloidal nanoparticles and SiO_2 precursor, resulting that smaller SiO_2 region could be formed compared to polymer solution without SiO_2 colloidal nanoparticles. Therefore, smaller pore size by SiO_2 precursor and large pore size by SiO_2 NPs could lead to largest surface area of MSP TiO_2 NFs compared with large pore TiO_2 and small pore TiO_2 NFs. Effect of pores on the light scattering was investigated by measuring the diffuse reflectance spectra (DRS) (see Figure S1 in the Supporting Information).

To determine the effect of TiO_2 NF morphology on the photovoltaic properties of DSSCs, we coated different TiO_2 NF layers with different pore types on highly transparent 15-20 nm TiO_2 nanoparticle films. As shown in Table 2, the surface area of MSP TiO_2 NFs was nine times larger than that of the SP and LP TiO_2 NFs. Pores made by removing the SiO_2 precursor played an important role in enhancing the surface area of TiO_2 NFs. The solution of SiO_2 colloidal nanoparticles and SiO_2 precursor provided the largest surface area. Moreover, a small amount of residue SiO_2 on the surface area of the TiO_2 could increase light scattering efficiency because difference of refractive index (n).The reflectance of anatase TiO_2 NFs (n_{TiO2} = 2.49) is higher than that of residue SiO_2 (n_{SiO2}= 1.47), leading to increase in the refractive index difference between the two materials and the surrounding matrix (n_{air} = 1.00), attributing to the increase in the scattering efficiency.[40] As a result, the conversion efficiency of MSP TiO_2 NFs was improved from 4.8% to 8.5% compared to that of TiO_2 NFs (Figure 5a). MSP TiO_2 NFs had the highest short-circuit current density (J_{sc}) of the TiO_2 NFs, which was probably related to the amount of adsorbed dye. Thus, dye uptake among TiO_2 NFs with different pore types should be considered. Dye uptake increased drastically with increasing surface area. The amount of adsorbed dye for the MSP TiO_2 NFs was 132.7 mol g^{-1}, which was approximately two times larger than for TiO_2 NFs (63.9 mol g^{-1}). The increased dye absorption on MSP TiO_2 NFs was due to their high surfaces area. Thus, pore size likely influences the efficiency of solar cells. The pore size of SP TiO_2 NFs was determined to be 6.7 nm when formed by a SiO_2 precursor. These pores were occupied by dye molecules (molecular diameter of 1.5 nm) that had adsorbed on the pore walls, leaving an aperture for electrolyte diffusion. The aperture was similar in size to an I_3^- ion; thus, Fick's law of diffusion was not valid. The diffusion kinetics in the electrolyte was the limiting step in the current production. On the other hand, MSP TiO_2 NFs consisted of pores with diameters of 6.7 nm and 28 nm. SPs can induce the adsorption of dye molecules, and LPs can increase the adsorption of dye molecules on the wall as well as facilitate electrolyte diffusion and circulation for regenerating sensitized dye molecules.[7] Thus, the MSP TiO_2 NFs could enhance the efficiency of DSSCs compared to SP TiO_2 NFs.

Figure 5b shows the IPCE spectra as a function of wavelength for the TiO_2 NFs. The IPCE of MSP TiO_2 NFs was higher than that of the other three samples over the entire

wavelength region, which is in good agreement with the observed higher J_{sc}. The difference in IPCE at shorter wavelengths may be attributable to different absorbed dye concentrations. The shape of IPCE spectra at long wavelengths was similar for all samples because of the similar light-scattering effect.[19]

In conclusions, we fabricated MSP TiO_2 NFs and investigated their photovoltaic performance in DSSCs. The surface area of the MSP TiO_2 NFs was nine times larger than that of SP and LP TiO_2 NFs, leading to enhanced adsorption of dye molecules. In addition, MSP TiO_2 NFs exhibited excellent light scattering. LPs in MSP TiO_2 NFs provide a place for circulation and facilitate electrolyte diffusion for oxidation reaction. By controlling the thickness of the photoanode layer, the conversion efficiency of MSP TiO_2 NFs was improved by up to 8.5%. Therefore, MSP TiO_2 NFs can be used as an efficient material for high-efficiency DSSCs. In addition, our approach enables the utilization of a porous structure in electrode materials, such as catalysts for various energy applications, rechargeable batteries, and supercapacitors.

■ ASSOCIATED CONTENT

Supporting Information

Additional figures (PDF). This material is available free of charge via the Internet at http://pubs.acs.org.

■ AUTHOR INFORMATION

Corresponding Author

*E-mail: jsjang@plaza.snu.ac.kr.

Notes

The authors declare no competing financial interest.

■ ACKNOWLEDGMENTS

This work was supported by Global Frontier R&D Program on Center for Multiscale Energy System funded by the National Research Foundation under the Ministry of Education, Science and Technology, Korea(2011-0031573) and WCU (World Class University) program through the National Research Foundation of Korea funded by the Ministry of Education, Science and Technology (R31-10013).

■ REFERENCES

(1) O'Regan, B.; Grätzel, M. *Nature* **1991**, *353*, 737−740.
(2) Grätzel, M. *Nature* **2001**, *414*, 338−344.
(3) Cho, S.; Hwang, S. H.; Kim, C.; Jang, J. *J. Mater. Chem.* **2012**, *22*, 12164−12171.
(4) Wang, Q.; Ito, S.; Grätzel, M.; Fabregat-Santiago, F.; Mora-Seró, I.; Bisquert, J.; Bessho, T.; Imai, H. *J. Phys. Chem. B* **2006**, *110*, 25210−25221.
(5) Grätzel, M. *Inorg. Chem.* **2005**, *44*, 6841−6851.
(6) Sauvage, F.; Chen, D.; Comte, P.; Huang, F.; Heiniger, L. P.; Cheng, Y. B.; Caruso, R. A.; Graetzel, M. *ACS Nano* **2010**, *4*, 4420−4425.
(7) Lee, Y. M.; Kim, Y. H.; Lee, J. H.; Park, J. H.; Park, N. G.; Choe, W. S.; Ko, M. J.; Yoo, P. J. *Adv. Funct. Mater.* **2011**, *21*, 1160−1167.
(8) Grinis, L.; Kotlyar, S.; Rühie, S.; Grinblat, J.; Zaban, A. *Adv. Funct. Mater.* **2010**, *20*, 282−288.
(9) Muduli, S.; Lee, W.; Dhas, V.; Mujawar, S.; Dubey, M.; Vijayamohanan, K.; Han, S. H.; Ogale, S. *ACS Appl. Mater. Interfaces* **2009**, *1*, 2030−2035.
(10) Hwang, D.; Lee, H.; Jang, S. Y.; Jo, S. M.; Kim, D.; Seo, Y.; Kim, D. Y. *ACS Appl. Mater. Interfaces* **2011**, *3*, 2719−2725.
(11) Cameron, P. J.; Peter, L. M. *J. Phys. Chem. B* **2003**, *107*, 14394−14400.
(12) Palomares, E.; Clifford, J. N.; Haque, S. A.; Lutz, T.; Durrant, J. R. *J. Am. Chem. Soc.* **2003**, *125*, 475−482.
(13) Hwang, S. H.; Song, J.; Jung, Y.; Kweon, O. Y.; Song, H.; Jang, J. *Chem. Commun.* **2011**, *47*, 9164−9166.
(14) Oh, W. K.; Kim, S.; Choi, M.; Kim, C.; Jeong, Y. S.; Cho, B. R.; Hahn, J. S.; Jang, J. *ACS Nano* **2010**, *4*, 5301−5313.
(15) Barbé, C. J.; Arendse, F.; Comte, P.; Jirousek, M.; Lenzmann, F.; Shklover, V.; Grätzel, M. *J. Am. Ceram. Soc.* **1997**, *80*, 3157−3171.
(16) Yu, H.; Xue, B.; Liu, P.; Qiu, J.; Wen, W.; Zhang, S.; Zhao, H. *ACS Appl. Mater. Interfaces* **2012**, *4*, 1289−1294.
(17) Sommeling, P. M.; O'Regan, B. C.; Haswell, R. R.; Smit, H. J. P.; Bakker, N. J.; Smits, J. J. T.; Kroon, J. M.; Van Roosmalen, J. A. M. *J. Phys. Chem. B* **2006**, *110*, 19191−19197.
(18) O'Regan, B. C.; Durrant, J. R.; Sommeling, P. M.; Bakker, N. J. *J. Phys. Chem. C* **2007**, *111*, 14001−14010.
(19) Wu, X.; Chen, Z.; Max, Lu, G. Q.; Wang, L. *Adv. Funct. Mater.* **2011**, *21*, 4167−4172.
(20) Wang, Z. S.; Kawauchi, H.; Kashima, T.; Arakawa, H. *Coord. Chem. Rev.* **2004**, *248*, 1381−1389.
(21) Ito, S.; Zakeeruddin, S. M.; Humphry-Baker, R.; Liska, P.; Charvet, R.; Comte, P.; Nazeeruddin, M. K.; Péchy, P.; Takata, M.; Miura, H.; Uchida, S.; Grätzel, M. *Adv. Mater.* **2006**, *18*, 1202−1205.
(22) Koo, H. J.; Kim, Y. J.; Lee, Y. H.; Lee, W. I.; Kim, K.; Park, N. G. *Adv. Mater.* **2008**, *20*, 195−199.
(23) Kang, T. S.; Smith, A. P.; Taylor, B. E.; Durstock, M. F. *Nano Lett.* **2009**, *9*, 601−606.
(24) Tan, B.; Wu, Y. *J. Phys. Chem. B* **2006**, *110*, 15932−15938.
(25) Ohsaki, Y.; Masaki, N.; Kitamura, T.; Wada, Y.; Okamoto, T.; Sekino, T.; Niihara, K.; Yanagida, S. *Phys. Chem. Chem. Phys.* **2005**, *7*, 4157−4163.
(26) Joshi, P.; Zhang, L.; Davoux, D.; Zhu, Z.; Galipeau, D.; Fong, H.; Qiao, Q. *Energy Environ. Sci.* **2010**, *3*, 1507−1510.
(27) Yang, L.; Leung, W. W. F. *Adv. Mater.* **2011**, *23*, 4559−4562.
(28) Law, M.; Greene, L. E.; Johnson, J. C.; Saykally, R.; Yang, P. *Nature Mater.* **2005**, *4*, 455−459.
(29) Gubbala, S.; Chakrapani, V.; Kumar, V.; Sunkara, M. K. *Adv. Funct. Mater.* **2008**, *18*, 2411−2418.
(30) Liu, B.; Aydil, E. S. *J. Am. Chem. Soc.* **2009**, *131*, 3985−3990.
(31) Lee, B. H.; Song, M. Y.; Jang, S. Y.; Jo, S. M.; Kwak, S. Y.; Kim, D. Y. *J. Phys. Chem. C* **2009**, *113*, 21453−21457.
(32) Saji, V. S.; Pyo, M. *Thin Solid Films* **2010**, *518*, 6542−6546.
(33) Sauvage, F.; Di Fonzo, F.; Li Bassi, A.; Casari, C. S.; Russo, V.; Divitini, G.; Ducati, C.; Bottani, C. E.; Comte, P.; Graetzel, M. *Nano Lett.* **2010**, *10*, 2562−2567.
(34) Zhuge, F.; Qiu, J.; Li, X.; Gao, X.; Gan, X.; Yu, W. *Adv. Mater.* **2011**, *23*, 1330−1334.
(35) Stöber, W.; Fink, A.; Bohn, E. *J. Colloid Interface Sci.* **1968**, *26*, 62−69.
(36) Park, N. G.; Van De Lagemaat, J.; Frank, A. J. *J. Phys. Chem. B* **2000**, *104*, 8989−8994.
(37) Koo, H. J.; Park, J.; Yoo, B.; Yoo, K.; Kim, K.; Park, N. G. *Inorg. Chim. Acta* **2008**, *361*, 677−683.
(38) Archana, P. S.; Jose, R.; Vijila, C.; Ramakrishna, S. *J. Phys. Chem. C* **2009**, *113*, 21538−21542.
(39) Knotter, D. M *J. Am. Chem. Soc.* **2000**, *122*, 4345−4351.
(40) Takano, Y.; Liou, K. N. *Appl. Opt.* **2010**, *49*, 3990−3996.